Michelle S. Hoo Fatt
Department of Naval Architecture and Offshore Engineering
University of California, Berkeley
Berkeley, CA 94720

Plastic Deformation and Rupture of Ring-Stiffened Cylinders under Localized Pressure Pulse Loading

An analytical solution for the dynamic plastic deformation of a ring-stiffened cylindrical shell subject to high intensity pressure pulse loading is presented. By using an analogy between a cylindrical shell that undergoes large plastic deformation and a rigid-plastic string resting on a rigid-plastic foundation, one derives closed-form solutions for the transient and final deflection profiles and fracture initiation of the shell. Discrete masses and springs are used to describe the ring stiffeners in the stiffened shell. The problem of finding the transient deflection profile of the central bay is reduced to solving an inhomogeneous wave equation with inhomogeneous boundary conditions using the method of eigenfunction expansion. The overall deflection profile consists of both global (stiffener) and local (bay) components. This division of the shell deflection profile reveals a complex interplay between the motions of the stiffener and the bay. Furthermore, a parametric study on a ring-stiffened shell damaged by a succession of underwater explosions shows that the string-on-foundation model with ring stiffeners described by lumped masses and springs is a promising method of analyzing the structure. © *1994 John Wiley & Sons, Inc.*

INTRODUCTION

Obtaining closed-form solutions for the structural response of a ring-stiffened cylindrical shell is not only a necessary step in understanding the design of ring stiffeners as strengthening mechanisms for the shell but also in studying the failure modes associated with the presence of the ring stiffeners when the shell is subjected to various loads. For instance, a ring-stiffened shell under asymmetric explosive-type loading may experience stiffener tripping, stiffener detachment, and so-called hard-point fracture (fracture of the base-plate of shell at the location of the stiffener web). The particular type(s) of failure mechanism would depend on the peak pressure and load duration. This article focuses only on the fracture of the base plate of the shell. Stiffener tripping and detachment have been studied by Huang and Wierzbicki (1993) and Giovanola and Kirkpatrick (1992), respectively.

The quest for analytical solutions of the large plastic deformation of a cylindrical shell under asymmetric pressure loading often leads to the derivation of a set of shell differential equations that are difficult to solve (Flugge, 1973). Because of the mathematical complexities involved in obtaining analytical solutions to these equations,

Orig. Received Nov. 26, 1992; Revised received Dec. 26, 1993.

Shock and Vibration, Vol. 1, No. 3, pp. 289–301 (1994)

CCC 1070-9622/94/030289-13

numerical methods, such as those implemented in DYNA, ABAQUS, and ADINA, have been used to solve many practical problems. Furthermore, very little analytical attempt has been made to incorporate ring stiffeners into the shell equations for the case of a ring-stiffened shell, although some attempts have been made with the use of computer codes (Stricklin et al., 1974).

Within recent years, a way of modeling the cylindrical shell undergoing large plastic deformation as a rigid-plastic string resting on a rigid-plastic foundation has given insight into the development of a closed-form solution for the structural behavior of a ring-stiffened shell. As a result of rigorously derived assumptions and simplifications of a cylindrical shell undergoing large plastic deformation, the model considers the only two dominant load-resisting mechanisms in the shell: stretching in the logitudinal direction and bending in the circumferential direction (Hoo Fatt, 1992). An averaging procedure in the circumferential direction of the shell is used to eliminate the spatial variable in the circumferential direction of the shell. This leads to the derivation of equivalent functions and reduces the problem to one-dimension. The membrane resistance in the axial direction and the circumferential bending resistance of the shell are represented by an equivalent tensile force and an equivalent foundation force in a string resting on a foundation, respectively. The equivalent functions are calculated from a stationary hinge ring model that describes the deformation of each section of the shell. It has been found that the equivalent functions vary weakly in the axial direction of the shell, and assuming that they are constant greatly simplifies the analysis with very little loss of accuracy (Hoo Fatt, 1992). Equivalent functions are henceforth called equivalent parameters (or constants). The complex two-dimensional problem is therefore reduced to a one-dimensional problem involving an inhomogeneous, partial differential equation in the axial direction and time. Closed-form solutions of related problems using this concept have already been derived (Hoo Fatt and Wierzbicki, 1992). The conclusion drawn from previous analyses is that the string-on-foundation model is a powerful model for predicting the transient plastic response of cylindrical shells undergoing impact and localized pressure loading.

Modeling a cylindrical shell first under axisymmetric loading as a beam-on-foundation originated in elastic shell theory (Den Hartog, 1952). The idea was further applied to elastic shells under asymmetric loads by Calladine (1977). Since then the analogy between the cylindrical shell and a beam-on-foundation has been used to solve various problems ranging from pinching of tubes (Reid, 1978) to projectile impact into thin cylindrical shells (Yu and Stronge, 1990). To account for even larger deformation of the shell, it has been proposed to replace the beam analogy by one of a string-on-foundation. According to finite-deflection theory, a rigid-plastic beam behaves like a string when deflections are of the order of the thickness of the beam (Gurkok and Hopkins, 1973). A beam under moderately large deflection is said to have reached its membrane state. Therefore, one would expect that the beam-on-foundation would behave more like a string-on-foundation once the shell has reached its large deflection state. Once the shell is modeled as a string-on-foundation, the solution for the transient deflection profiles of the shell is determined by solving an inhomogeneous wave equation, with initial-boundary conditions that depend on the specified loading conditions.

Because ring stiffeners only add to the circumferential bending resistance of the shell, they are incorporated into the string-on-foundation model as additional foundation resistance and represented by discrete rigid-plastic springs with associated stiffnesses and masses. The deformation of the central bay and its adjacent stiffeners may then be examined by formulating equilibrium on a local scale. Shear forces are transmitted at the interface of the bay and the stiffener and the transmission of shear force is expressed in one of the boundary conditions for the partial differential equation.

The purpose of this article is to present a closed-form solution for the transient and final deflection profiles of the central bay of the stiffened shell. The problem formulation is briefly summarized here. One may find a more detailed account of the assumptions and simplifications that lead to the string-on-foundation model in Hoo Fatt (1992). Furthermore, the maximum strains within the central bay are calculated in order to introduce a simple fracture criterion based on the critical strain to rupture the shell. Theoretical calculations are based on the geometry and loading of a damaged ring-stiffened shell subject to a series of underwater explosions (McDonald, 1992). A parametric study helps to establish the validity of the model.

PROBLEM FORMULATION

Consider an infinite cylindrical shell of radius R and thickness h, with ring stiffeners equally spaced apart by a distance $2l$, as shown in Fig. 1. The shell material is idealized as rigid, perfectly plastic with flow stress σ_o. The cylinder is subjected to an applied pressure load $p(x, \theta, t)$ and undergoes radial deformation $w(x, \theta, t)$, where x, θ denotes the axial and circumferential coordinates and t denotes time.

In general, the shell is loaded by an inward radial pressure $p(x, \theta, t)$. The size of the "patch" load is of the order of the shell radius or smaller so that the resulting deformations are highly localized. As shown in Fig. 1, the pressure distribution is assumed to have two planes of symmetry, at $x = 0$ and at $\theta = 0$, and a variable amplitude but a fixed shape. The pressure amplitude rises instantaneously to the maximum value p_o and then decays exponentially with a characteristic time constant τ, according to

$$p(x, \theta, t) = p_o e^{-(t/\tau)} h(x) g(\theta), \tag{1}$$

where $h(x)$ and $g(\theta)$ are known, dimensionless shape functions.

The overall shell equilibrium is expressed via the principle of virtual velocities. It was shown in Hoo Fatt (1992) that plastic work dissipated by the shell under large plastic deformation consisted of only two significant terms, membrane stretching energy W_m in the axial direction and circumferential bending energy W_b. Given a rigid-plastic material assumption, a limited interaction yield curve, and a Lagrangian coordinate description, these two energy terms are defined by

$$\dot{W}_m = 2 \int_0^{\xi} 2R \int_0^{\pi} |N_{\text{pl}} w' \dot{w}'| d\theta \, dx \tag{2}$$

and

$$\dot{W}_b = 2 \int_0^{\xi} 2R \int_0^{\pi} |M_{\text{pl}} \dot{\kappa}_{\theta\theta}| d\theta \, dx, \tag{3}$$

where ξ is the length of the deformed shell, $\dot{\kappa}_{\theta\theta}$ is the circumferential curvature rate, and N_{pl} and M_{pl} are the fully plastic membrane force and bending moment per unit length of the shell, respectively. Note that the axial component of the longitudinal strain rate in Eq. (2) is neglected.

Therefore, the global shell equilibrium equation is

$$\begin{aligned} \bar{T}\dot{w}|_{\text{ends}} + 2 \int_0^{L} 2R \int_0^{\pi} p\dot{w} d\theta \, dx \\ = 2 \int_0^{\xi} 2R \int_0^{\pi} |M_{\text{pl}} \dot{\kappa}_{\theta\theta}| d\theta \, dx \\ + 2 \int_0^{\xi} 2R \int_0^{\pi} N_{\text{pl}} w' \dot{w}' d\theta \, dx \\ + 2 \int_0^{\xi} 2R \int_0^{\pi} m(\ddot{w}\dot{w} + \ddot{v}\dot{v}) \, d\theta \, dx, \end{aligned} \tag{4}$$

where L is the extent of the load on both sides of the symmetry plane, $\bar{T}$ is a shear force applied at the end of the deformed shell, and m is the mass per unit length of the shell. The thickness h in the ring-stiffened shell varies in a price-wise manner along the x-axis so that both M_{pl} and m are functions of position x.

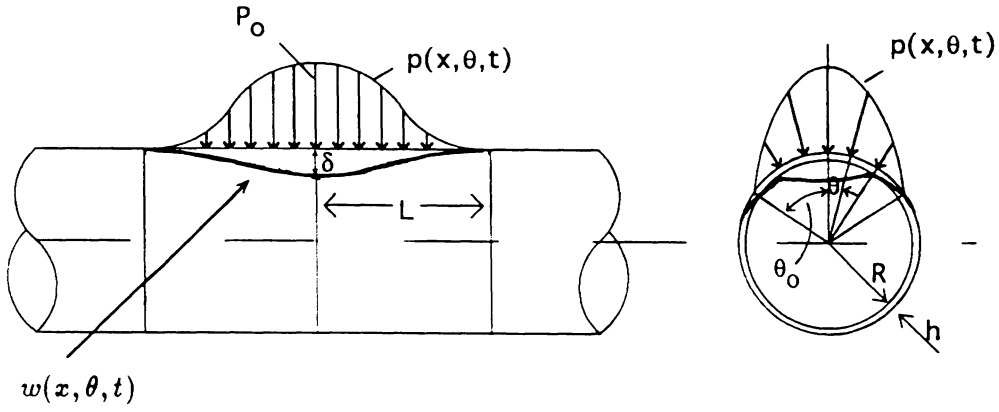

FIGURE 1 Geometry and loading of a cylindrical shell.

Equation (4) is integrated in the θ direction to give

$$\bar{T}\dot{w}|_{\text{ends}} + 2\int_0^L \bar{p}\dot{w}\,dx = 2\int_0^\xi \bar{q}\dot{w}\,dx + 2\int_0^\xi \bar{N}w'\dot{w}'\,dx + 2\int_0^\xi \bar{m}\ddot{w}\dot{w}\,dx, \quad (5)$$

where the following equivalent functions are introduced: an equivalent line load,

$$\bar{p}(x,t)\dot{w}(x,0,t) = 2R\int_0^\pi p(x,\theta\,t)\,\dot{w}(x,\theta,t)\,d\theta; \quad (6)$$

an equivalent bending resistance,

$$\bar{q}(x,t)\dot{w}(x,0,t) = 2R\int_0^\pi |M_{\text{pl}}\dot{\kappa}_{\theta\theta}|\,d\theta; \quad (7)$$

an equivalent tensile force,

$$\bar{N}\dot{w}'(x,0,t)\,\dot{w}'(x,0,t) = 2RN_{\text{pl}}\int_0^\pi w'\dot{w}'(x,\theta,t)\,d\theta; \quad (8)$$

an equivalent mass per unit length,

$$\bar{m}\ddot{w}(x,0,t)\,\dot{w}(x,0,t) = 2Rm\int_0^\pi (\ddot{w}\dot{w} + \ddot{v}\dot{v})(x,\theta,t)\,d\theta. \quad (9)$$

Note that all the deformation in the circumferential direction is lumped into the deflection at $\theta = 0$ so that from here on, w will be a function of only x and t.

Integration in the circumferential direction is performed once a velocity field in the circumferential direction of the shell is known. This velocity field is found by developing a stationary hinge ring model that gives a realistic deformation pattern for the collapse of each ring. The stationary hinge ring model shown in Fig. 2 describes the collapse mechanism for this problem and is used to calculate the equivalent parameters. The derivation of equivalent parameters is a straightforward process, but it involves long and tedious algebra in evaluating the integrals in Eqs. (6)–(9). The equivalent functions are derived in Hoo Fatt (1992) and summarized in Table 1.

Integrating Eq. (5) by parts, one gets

$$(\bar{T} - 2\bar{N}w')\dot{w}|_{\text{ends}} + 2\int_0^\xi (\bar{m}\ddot{w} - \bar{N}w'' + \bar{q} - \bar{p})\dot{w}\,dx = 0, \quad (10)$$

where $\bar{T}$ represents an applied shear force at the end. From variational calculus, the system is re-

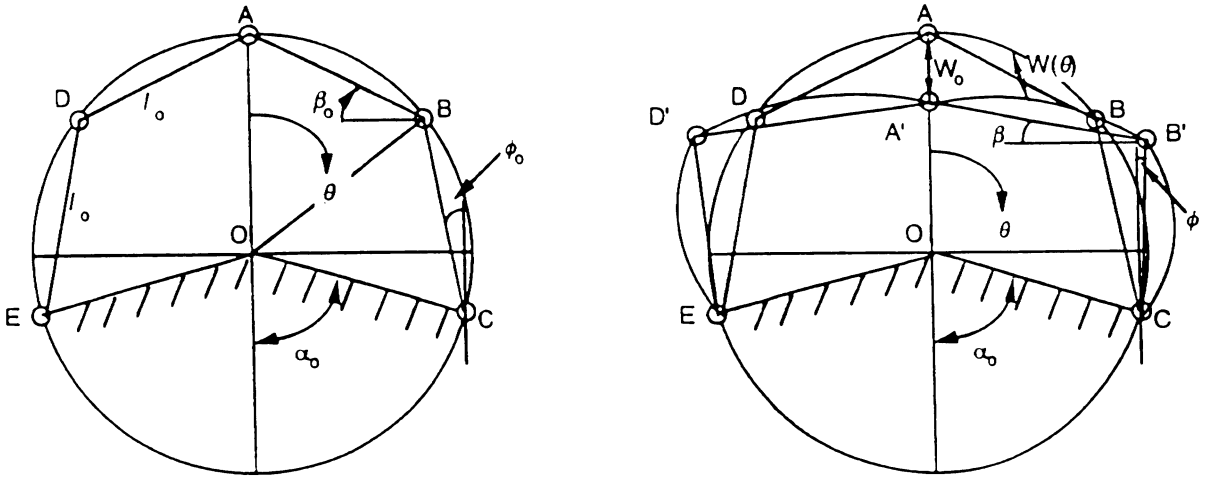

A. Undeformed B. Deformed

FIGURE 2 Stationary hinge ring model.

Table 1. Equivalent Parameters

Parameter	Definition	Calculated Value
$\bar{p}$	$\bar{p}(x, t)\dot{w}(x, 0, t) = 2R\int_0^\pi p(x, \theta, t)\dot{w}(x, \theta, t)\, d\theta$	$0.5Rp_o$
$\bar{q}$	$\bar{q}(x, t)\dot{w}(x, 0, t) = 2R\int_0^\pi \lvert M_{pl}\dot{\kappa}_{\theta\theta}\rvert d\theta$	$8M_{pl}/R$
$\bar{N}$	$\bar{N}\dot{w}'(x, 0, t)\dot{w}'(x, 0, t) = 2RN_{pl}\int_0^\pi w'\dot{w}'(x, \theta, t)\, d\theta$	$0.5N_{pl}R$
$\bar{m}$	$\bar{m}\ddot{w}(x, 0, t)\dot{w}(x, 0, t) = 2Rm\int_0^\pi \ddot{w}\dot{w}(x, \theta, t)\, d\theta$	$0.5mR$

duced to the following partial differential equation:

$$\bar{m}\ddot{w} - (\bar{N}w')' + \bar{q} - \bar{p} = 0 \tag{11}$$

subject to the boundary conditions

$$w' = 0 \quad \text{at} \quad x = 0 \tag{12}$$

and

$$2\bar{N}w' = \bar{T} \quad \text{at} \quad x = \xi. \tag{13}$$

Equation (11) is also subject to the initial conditions

$$w = 0 \quad \text{at} \quad t = 0 \tag{14}$$

and

$$\dot{w} = 0 \quad \text{at} \quad t = 0. \tag{15}$$

Pressure pulse loading with high peak pressures and short durations can be replaced by impulsive loading so that $\bar{p} = 0$ in Eq. (11) and $\dot{w}(x, 0) = \bar{I}f(x)$, where $\bar{I}$ is related to both the maximum pressure amplitude p_o and decay constant τ of a pressure pulse shock wave and $f(x)$ is a shape function used to describe the initial velocity distribution. The advantage of replacing the pressure load by an impulse load is a one parameter representation of the pressure load. Equations (11)–(15) represent an initial-boundary value problem for an inhomogeneous wave equation.

If ring stiffeners are to be incorporated into the string-on-foundation model, they must be represented as discrete bending resistance forces or discrete plastic springs with lumped masses $\bar{M}$ and stiffnesses $\bar{Q}$. The lumped mass of the stiffener $\bar{M}$ is defined in terms of the local shell coordinates so that $dA = dx\, dz$

$$\dot{w}\ddot{w}\bar{M} = \int_A \rho dA[2R\int_0^\pi (\dot{w}\ddot{w} + \dot{v}\ddot{v})\, d\theta]. \tag{16}$$

The integral for the ring resistance $\bar{Q}$ involves the distance z from the neutral axis

$$\dot{w}\bar{Q} = \int_A \sigma_o z\, dA[2R\int_0^\pi \dot{\kappa}_{\theta\theta}\, d\theta]. \tag{17}$$

With these definitions, $\bar{M}$ and $\bar{Q}$ would depend on the geometry of the stiffener.

Equilibrium may now be imposed on a more local sense by writing the principle of virtual work between stiffeners or for each separate bay. The pressure distribution within each bay may be considered approximately constant. Attention is focused on the transient deflection of the central bay because it is here that fracture is most likely to occur. Thus, for the central bay

$$\bar{m}\ddot{w} - \bar{N}w'' + \bar{q} - \bar{p} = 0, \tag{18}$$

with boundary conditions

$$w' = 0 \quad \text{at} \quad x = 0 \tag{19}$$

and

$$\bar{N}w' = \bar{T} = -(\bar{Q} + \bar{M}\ddot{w})/2 \quad \text{at} \quad x = l, \tag{20}$$

where $\bar{T} = -(\bar{Q} + \bar{M}\ddot{w})/2$ is the shear force on the half bay and half of the stiffener. The solution for the deformation within the central bay is coupled with that for the stiffener via the boundary conditions.

The initial conditions to Eq. (18) are as follows

$$w = 0 \quad \text{at} \quad t = 0 \tag{21}$$

and

$$\dot{w} = \bar{I}f(x) \quad \text{at} \quad t = 0. \tag{22}$$

The boundary condition at $x = l$ shows the coupling associated with the bay and the stiffener. The stiffener is modeled as a discrete system with lumped mass $\bar{M}$ and foundation resistance $\bar{Q}$ subject to a forcing input that is equal to

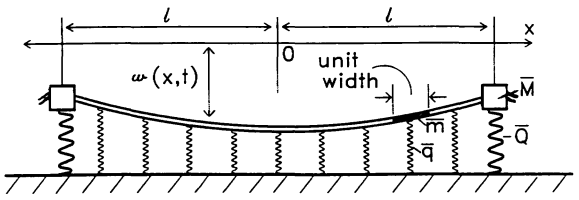

FIGURE 3 A continuous-discrete model of a single bay in the ring-stiffened shell.

the shear force transmitted from the motion of the bay. Formulating the principle of virtual velocities for the central bay has therefore enabled us to view the complex two-dimensional problem as the two coupled subsystems shown in Fig. 3.

SOLUTION OF THE PARTIAL DIFFERENTIAL EQUATION

The initial-boundary value problem is defined in the following normalized coordinate system:

$\tilde{x} = x/l$	axial coordinate
$\tilde{t} = tc/l$	time
$\tilde{I} = \bar{I}\bar{N}/cl\bar{q}$	impulse velocity
$\tilde{w} = w\bar{N}/l^2\bar{q}$	transverse deflection
$\eta = \bar{M}/\bar{m}l$	mass ratio
$\zeta = \bar{Q}/\bar{q}l$	stiffness ratio
$\tilde{f} = \bar{T}/\bar{q}l$	shear force
$\tilde{p} = \bar{p}/\bar{q}$	line load amplitude.

In terms of these dimensionless quantities, Eqs. (18)–(22) reduce to

$$\tilde{w}_{\tilde{t}\tilde{t}} - \tilde{w}_{\tilde{x}\tilde{x}} + 1 = 0, \tag{23}$$

with boundary conditions

$$\tilde{w}_{\tilde{x}} = 0 \quad \text{at} \quad \tilde{x} = 0 \tag{24}$$

and

$$\tilde{w}_{\tilde{t}\tilde{t}} + \frac{2}{\eta}\tilde{w}_{\tilde{x}} + \frac{\zeta}{\eta} = 0 \quad \text{at} \quad \tilde{x} = 1, \tag{25}$$

and initial conditions

$$\tilde{w} = 0 \quad \text{at} \quad \tilde{t} = 0 \tag{26}$$

and

$$\tilde{w}_{\tilde{t}} = \tilde{I}f(\tilde{x}) \quad \text{at} \quad \tilde{t} = 0. \tag{27}$$

Insight from Kelly and Wierzbicki (1967) as well as an attempt to solve the problem using the method of characteristics reveal that the solution is of the form

$$\tilde{w} = \bar{w} + \alpha_1(1 - \tilde{x}^2) + \beta_1\tilde{t}^2, \tag{28}$$

where $\bar{w}$ is the solution to the homogeneous wave equation. The inhomogeneous terms in the partial differential equation and the boundary condition at $\tilde{x} = 1$ are removed if

$$\alpha_1 = \frac{(\zeta - \eta)}{2(2 + \eta)} \tag{29}$$

and

$$\beta_1 = \frac{-(2 + \zeta)}{2(2 + \eta)}. \tag{30}$$

The homogeneous initial-boundary value problem is solved using the method of Fourier series expansion

$$\begin{aligned}\tilde{w} = {} & \lambda_0 F_0\tilde{t} + G_0 + \sum_{n=1}^{\infty}[F_n \sin(\lambda_n\tilde{t}) \\ & + G_n \cos(\lambda_n\tilde{t})]\cos(\lambda_n\tilde{x}) \\ & + \alpha_1(1 - \tilde{x}^2) + \beta_1\tilde{t}^2,\end{aligned} \tag{31}$$

where λ_n are the eigenvalues and $\cos \lambda_n\tilde{x}$ forms a complete set of symmetric orthogonal functions with respect to a special orthogonality condition.

Satisfying the boundary condition at $\tilde{x} = 1$ gives the eigenvalue equation

$$\tan \lambda_n = -\frac{\eta}{2}\lambda_n. \tag{32}$$

The first eigenvalue is the trivial case, $\lambda_0 = 0$. All other eigenvalues depend on the mass ratio η. The initial conditions to the partial differential equation specify the coefficients of F_n and G_n. Note that the boundary condition at $\tilde{x} = 1$ relates the acceleration to the slope and leads to an important modification of the orthogonality condition

$$\int_0^1 \tilde{w}_n\tilde{w}_m\,dx + \frac{\eta}{2}\tilde{w}_n(1)\tilde{w}_m(1) = 0, \tag{33}$$

where $n \neq m$.

On satisfying the initial conditions specified by Eqs. (26) and (27), one gets

$$G_0 + \sum_{n=1}^{\infty} G_n \cos(\lambda_n \bar{x}) = -\alpha_1(1 - \bar{x}^2) \quad (34)$$

and

$$\lambda_0 F_o + \sum_{n=1}^{\infty} \lambda_n F_n \cos(\lambda_n \bar{x}) = \bar{I} f(\bar{x}). \quad (35)$$

Expressions for G_n and $\lambda_n F_n$ using the special orthogonality condition specified by Eq. (33), are

$$G_0 = \frac{-4\alpha_1}{3(2 + \eta)}, \quad (36)$$

$$G_n = \frac{4\alpha_1(2 + \eta) \cos \lambda_n}{\lambda_n^2(2 + 3\eta \cos^2\lambda_n)}, \quad (37)$$

$$\lambda_0 F_o = \frac{2\bar{I}\left[\int_0^1 f(\bar{x})\, d\bar{x} + \frac{\eta}{2} f(1)\right]}{(2 + \eta)}, \quad (38)$$

and

$$\lambda_n F_n = \frac{2\bar{I}\left[\int_0^1 f(\bar{x}) \cos(\lambda_n \bar{x})\, d\bar{x} + \frac{\eta}{2} \cos \lambda_n f(1)\right]}{\left(1 + \frac{\sin(2\lambda_n)}{2\lambda_n} + \eta \cos^2 \lambda_n\right)}. \quad (39)$$

Note that the coefficients $\lambda_n F_n$ depend on the value of $f(1)$.

UNLOADING

Given the rigid-plastic string-on-foundation model, deformation reaches its final state when the velocity vanishes, $\dot{w} = 0$. However, tensile forces in the shell may start to unload before the velocity vanishes if $\dot{\varepsilon} = 0$. A more mathematical description of these two events may be given in a phase diagram (graph of t vs. x) as the $\mathcal{L}$- and $\mathcal{U}$-boundary, respectively. Several unloading possibilities can be distinguished, and they are summarized as follows:

If in the interval $0 < x < 1$,

1. $\dot{w} = 0$ occurs before $\dot{\varepsilon} = 0$ for all x (the unloading path is described by the $\mathcal{L}$-boundary), then every point in the bay reaches final deflection when $\dot{w} = 0$.
2. $\dot{w} = 0$ occurs before $\dot{\varepsilon} = 0$ for some but not all x (the $\mathcal{L}$- and $\mathcal{U}$-boundaries intersect at some points), then the solution for the final deformation profile becomes complicated because two unloading criteria will have to be used in finding the permanent deflection profile.
3. $\dot{\varepsilon} = 0$ before $\dot{w} = 0$ for all x (the $\mathcal{U}$-boundary is met before the $\mathcal{L}$-boundary), then local deflection ceases while global deformation continues. Unloading always starts at $x = 0$ and propagates toward the stiffener at $x = l$. Local motion ceases because the tensile forces N in the bay are less than the fully plastic tensile force $\bar{N}$ so that no additional stretching can take place. The bay must move, therefore, as a rigid body with constant but reduced tensile force N. When this happens, the deformed shell enters Phase II corresponding to rigid body translation of the string. Phase I is used to describe the deformation history before any unloading takes place. Phase II unloading will be pursued in the next section where a two-term Fourier series approximation for the transient deformation of the shell is used.

EXAMPLE

The proposed methodology is now applied to an actual ring-stiffened cylinder that was subject to a series of underwater explosive or shock wave loading over its entire length $L = 165$ in. It should be mentioned that the same problem has also been solved using modal analysis in Hoo Fatt (1992). Figure 4 shows some experimental profiles of a ring-stiffened cylindrical shell resulting from three consecutive underwater explosions (McDonald, 1992). The second and the third explosions act on an already damaged shell and only the results from the first explosion are relevant to this analysis because it is based on the undamaged shell. Note that after the third explosion, the shell undergoes very large deformation and ruptures. The shell and stiffener dimensions are shown in Fig. 5.

The pressure distribution resulting from the stand-off explosion is assumed by

$$p(x, \theta, t) = p_o e^{-(t/\tau)} \cos^2\left(\frac{\pi x}{2L}\right) g(\theta), \quad (40)$$

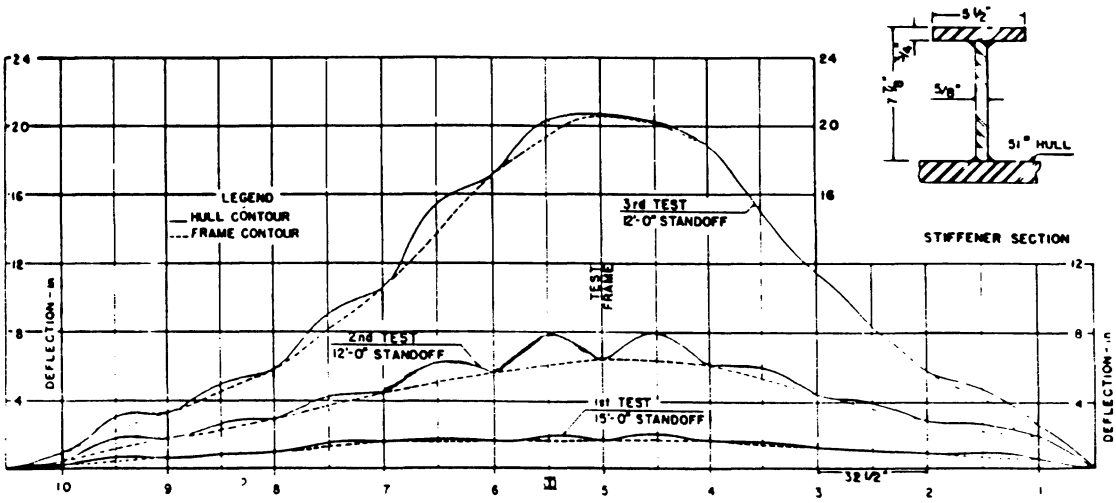

FIGURE 4 Experimental profiles.

where the magnitudes of p_o and τ for each explosion are given in Table 1. The material flow stress σ_o is 52,200 psi and the density ρ is 0.27 lbm/in^3. Although the amplitude of the pressure distribution varies in x, it is roughly constant between stiffeners. A constant local pressure amplitude in the central bay is given by

$$P_l = \frac{p_o}{l}\int_0^l \cos^2\left(\frac{\pi x}{2L}\right) dx. \tag{41}$$

The mass $\bar{M}$ and bending resistance $\bar{Q}$ of the stiffener were evaluated for the T-stiffener in

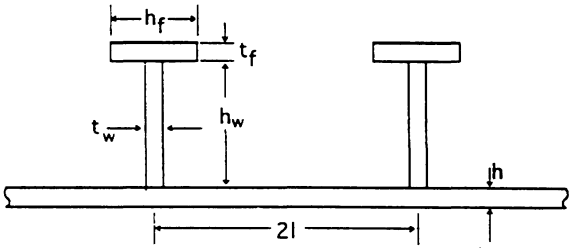

Shell dimensions

R	h	L	l
101.5in	1.25 in	165.0in	16.25 in

Dimensions of T-stiffener

t_w	h_w	h_f	t_f
0.625in	7.125 in	5.5 in	0.75 in

FIGURE 5 Stiffener dimensions.

Hoo Fatt (1992). These values together with other calculated values for the shell are given in Table 2.

A parabolic shape function is assumed for the shape of the initial velocity distribution $f(x)$

$$\dot{w} = \bar{I}[1 - (x/l)^2] \quad \text{at} \quad t = 0, \tag{42}$$

where $\bar{I}$ is the amplitude of the velocity calculated so that the total momentum imparted to the shell is equal to the initial shell momentum calculated for a parabolic velocity distribution. A parabolic distribution in the initial velocity is assumed because it is expected that the initial velocity would be small at the stiffener. This is because stiffeners usually have greater mass than the bay and would, therefore, have more initial inertial resistance. Hence, the initial velocity at the stiffener is much less than at the center of the bay. As a consequence of the initial velocity distribution specified in Eq. (42), one finds that $f(1) = 0$ and that the coefficients for F_n are related to those of G_n by

$$\lambda_n F_n = \frac{-G_n \bar{I}}{\alpha_1}. \tag{43}$$

Table 2. Pressure Loadings

Explosion No.	p_o (psi)	τ (ms)
1	6359.0	0.367
2	8209.0	0.348
3	8209.0	0.348

Table 3. Calculated Quantities for the Shell

$\bar{m}$	$\bar{M}$	$\bar{q}$	$\bar{Q}$	$\bar{N}$	Θ_0	η	ζ	$\tilde{I}$
15.38 lbm/in	361.64 lbm	1607.14 lb/in	94588.01 lb	3,467,729.24 lb	1.5	1.45	3.62	17.95

Note that the calculated value of η in Table 3 is 1.45 so that the mass of the stiffener is only 45% greater than that of the bay. The assumption of a parabolic distribution for the initial velocity (zero initial velocity at the stiffener) should therefore lead so some inaccuracies of the model. In a more refined model, a finite velocity would occur at the stiffener. The first 10 eigenvalues calculated for a chosen mass ratio $\eta = 1.45$ are given in Table 4.

Phase I: Motion Before Unloading

It was found that a two-term approximation ($n = 0, 1$) of the solution for the transverse deflections converges rapidly because the Fourier coefficients G_n are inversely proportional to λ_n^2 [see Eq. (37)], and a good approximation (within 15% for the value of the maximum central deflection) is

$$\tilde{w} = F_0\lambda_0\tilde{t} + G_0 + [F_1 \sin(\lambda_1\tilde{t}) + G_1 \cos(\lambda_1\tilde{t})] \cos(\lambda_1\tilde{x}) + \alpha_1(1 - \tilde{x}^2) + \beta_1\tilde{t}^2. \tag{44}$$

The velocity is then

$$\tilde{w}_{\tilde{t}} = F_0\lambda_0 + [F_1\lambda_1 \cos(\lambda_1\tilde{t}) - G_1\lambda_1 \sin(\lambda_1\tilde{t})] \cos(\lambda_1\tilde{x}) + 2\beta_1\tilde{t}. \tag{45}$$

This two-term approximation greatly simplifies the unloading analysis because the condition that $\dot{\varepsilon} = 0$ always occurs before $\dot{w} = 0$ (i.e., Case 3) and unloading will take place instantaneously at a critical time $\tilde{t}_c$. The $\mathcal{U}$-unloading boundary occurs instantaneously at

$$\tilde{t}_c = \frac{1}{\lambda_1} \tan^{-1}\left(\frac{-\tilde{I}}{\lambda_1\alpha_1}\right). \tag{46}$$

This type of unloading leads to rigid body translation because no additional extensional plastic deformation can take place within the bay. For $\tilde{t} > \tilde{t}_c$, motion in Phase II begins.

The normalized transient deflection and velocity profiles for the central bay in Phase I that result after the first explosion are shown in Figs. 6 and 7. The local deflections increase more rapidly than the global deflection at the stiffener in Phase I because a greater initial velocity is given to the bay than to the stiffener. Note that the initial velocity distribution in Fig. 7 is not precisely a parabolic function as a consequence of the two-term approximation.

Phase II: Motion After Unloading

For simplicity, equations for rigid body deflection are derived in physical variables and will later be represented in normalized coordinates. If the rigid body deformation of the bay in Phase II is denoted w_b, the new equation of motion for the bay is

$$\bar{m}l\ddot{w}_b - Nw_c' + \bar{q}l = 0, \tag{47}$$

where w_c' is a constant and depends on the solution of the previous analysis, $w_c' = w'(l, t_c)$, and $N < \bar{N}$ is the new value of the tensile force. Note that Eq. (47) is no longer a partial but a second order ordinary differential equation in time t because w_b is only a function of t. At $t = t_c$, the velocity is given by $\dot{w}_b(t_c) = \dot{w}(l, t_c)$. The final deflection and velocity in Phase I provides initial deflection and velocity in Phase II.

The boundary condition imposed at $x = l$ can also be interpreted as rigid body motion of the stiffener. Therefore, the equation of motion of

Table 4. First 10 Eigenvalues Calculated for Mass Ratio $\eta = 1.45$

λ_0	λ_1	λ_2	λ_3	λ_4	λ_5	λ_6	λ_7	λ_8	λ_9
0	2.14	4.98	8.02	11.1	14.2	17.3	20.4	23.6	26.7

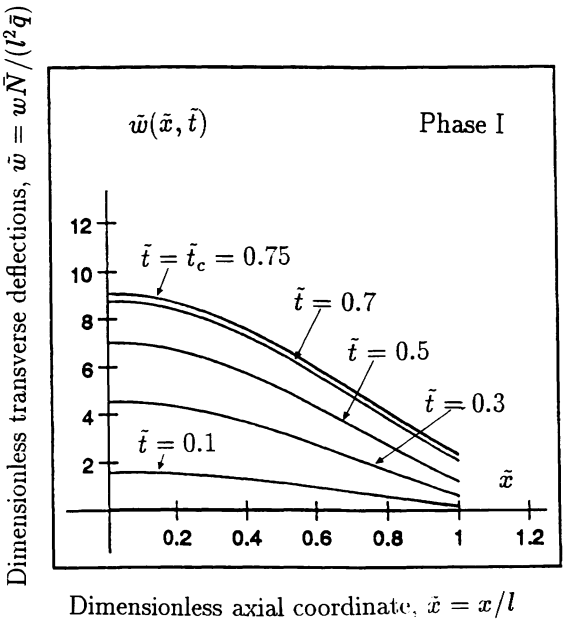

FIGURE 6 Normalized transient deflection profiles within the central bay.

the stiffener in Phase II is

$$\bar{M}\ddot{w}_b + \bar{Q} + 2Nw_c' = 0. \tag{48}$$

Eliminating $\ddot{w}_b$ from Eqs. (47) and (48) gives

$$N = \frac{(\bar{M}\bar{q} - \bar{m}\bar{Q})l}{(\bar{M} + 2\bar{m}l)w_c'} \tag{49}$$

or in normalized coordinates,

$$N = \frac{(\eta - \zeta)}{(2 + \eta)\tilde{w}_c'}\bar{N}. \tag{50}$$

The tensile force between bay and stiffener adjusts itself to a constant value N. A necessary condition for the development of Case 3 ($\dot{\varepsilon} = 0$ before $\dot{w} = 0$) is that $N < \bar{N}$ or $(\eta - \zeta)/(2 + \eta)\tilde{w}_c' < 1$.

Equation (49) is substituted into either Eqs. (47) or (48), and $\ddot{w}_b$ is integrated twice with respect to time to give in normalized coordinates

$$\tilde{w}_b = \frac{-(2 + \zeta)}{2(2 + \eta)}\tilde{t}^2 + b_1\tilde{t} + b_2, \tag{51}$$

where b_1 and b_2 are evaluated at the end of Phase I such that

$$b_1 = \tilde{w}_{\tilde{t}}(\tilde{t}_c) = \lambda_0 F_0 + \frac{[2\beta_1(2 + \eta) + 2 + \zeta]}{(2 + \eta)}\tilde{t}_c \tag{52}$$

and

$$b_2 = \tilde{w}(\tilde{t}_c) = G_0 - \frac{[2\beta_1(2 + \eta) + 2 + \zeta]}{2(2 + \eta)}\tilde{t}_c^2 + \cos\lambda_1\sqrt{(G_1^2 + F_1^2)}. \tag{53}$$

A PARAMETRIC STUDY

The simple model is further analyzed by performing a parametric study on a few chosen parameters. These parameters include the impulse velocity $\bar{I}$, which incorporates both the pressure amplitude and time constant; the bending resistance of the stiffener $\bar{Q}$; and the mass of the stiffener $\bar{M}$.

It is first necessary to represent both the final local and global deflections in terms of the normalized parameters $\tilde{I}$, η, and ζ. The final global deflection occurs at $\tilde{t} = \tilde{t}_f$, where $\tilde{t}_f$ is given by

$$\tilde{t}_f = \frac{b_1(\eta + 2)}{(2 + \zeta)}. \tag{54}$$

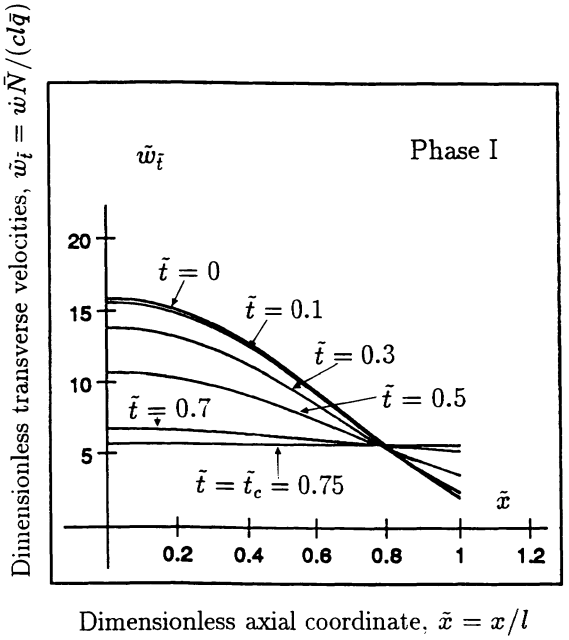

FIGURE 7 Normalized transient velocity profiles within the central bay.

Hence, the final global deflection $\tilde{\delta}_{gf}$ is

$$\tilde{\delta}_{gf} = \frac{b_1^2(\eta + 2)}{2(2 + \zeta)} + b_2, \tag{55}$$

where b_1 and b_2 are defined in Eqs. (52) and (53). Note that $\tilde{\delta}_{gf}$ will depend directly on $\tilde{I}$, and vary with η and ζ in a complicated manner.

On the other hand, the final local deflection $\tilde{\delta}_{lf}$ occurs at $\tilde{t} = \tilde{t}_c$ or at the end of Phase I and is given by

$$\tilde{\delta}_{lf} = \alpha_1 + \frac{4(2 + \eta)\cos\lambda_1(1 - \cos\lambda_1)\sqrt{(\tilde{I}^2 + \lambda_1^2\alpha_1^2)}}{\lambda_1^3(2 + 3\eta\cos^2\lambda_1)}. \tag{56}$$

Again $\tilde{\delta}_{lf}$ will depend on $\tilde{I}$, η, and ζ.

Figures 8–10 show how the maximum global and local deflections vary for the impulse parameter $\tilde{I}$, mass parameter η, and stiffness parameter ζ, respectively. The calculated values of ζ and η are not totally independent of each other because they both depend on the geometric and material properties of the ring-stiffened shell. The stiff-

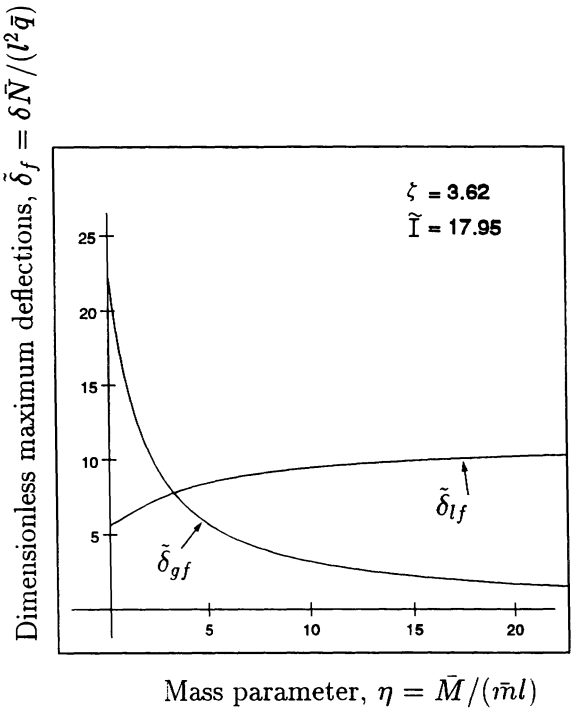

FIGURE 9 Maximum deflection versus mass parameter.

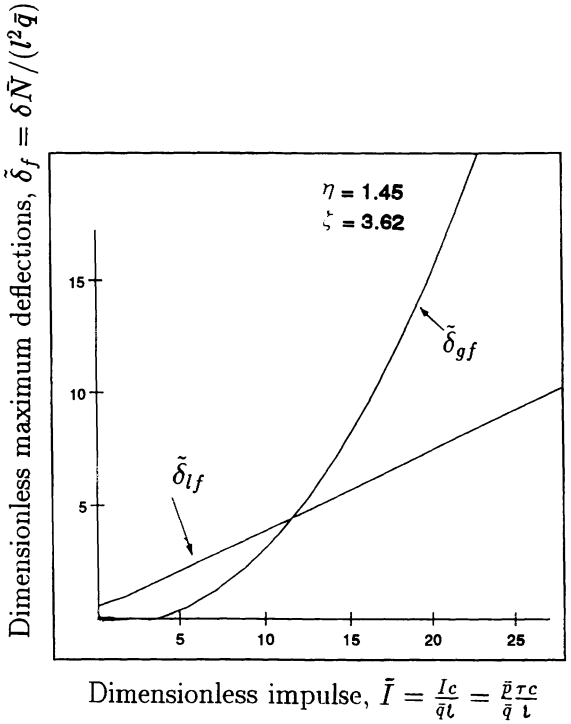

FIGURE 8 Maximum deflection versus impulse parameter.

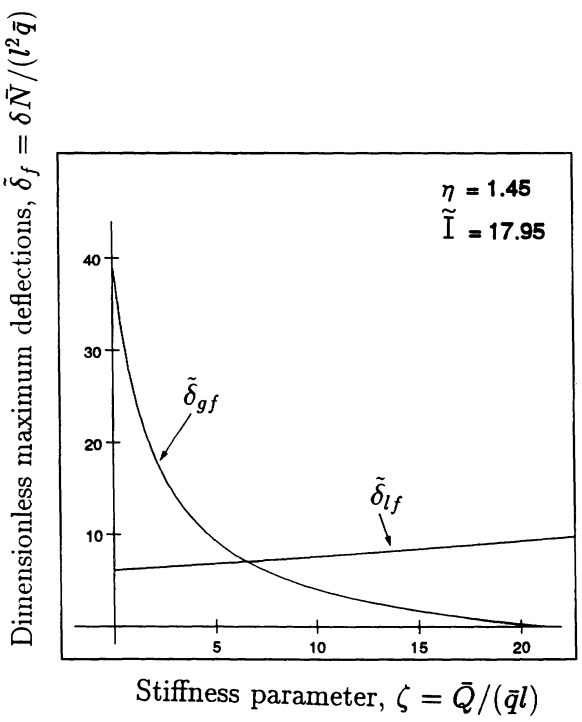

FIGURE 10 Maximum deflection versus stiffness parameter.

ness parameter ζ is directly proportional to σ_o, the mass parameter η is proportional to ρ, and both depend on the shape of the stiffener. However, for the purpose of a parametric study, each will be fixed while the other is allowed to vary.

As shown in Fig. 8, both local and global deflections increase with increasing impulse loading for the given ring-stiffened shell. A minimum impulse is needed to start global motion, and global deflections increase more rapidly than local deflections for greater impulse values. A minimum impulse is necessary to create tensile forces large enough to drive the stiffener mechanism.

In contrast to Fig. 8, the variation in local and global deflections are not the same for increasing mass parameter. With the applied impulse $\tilde{I}$ and ζ parameters constant, Fig. 9 shows how the maximum deflections vary for different values of η. As the stiffeners become heavier with respect to the bay (increasing η), local deformations are more pronounced while global deflections diminish.

Finally, the variation of global and local deformation with stiffness parameter is studied in Fig. 10. Again the impulse $\tilde{I}$ and mass parameter η are kept constant, while the stiffness parameter ζ is allowed to vary. When $\zeta = 0$, the stiffener has no resistance to bending and the global deformation is a maximum. Theoretically, local deflections should be negligible at $\zeta = 0$, but this is not shown in Fig. 10 because the mass of the stiffeners is fixed at $\eta = 1.45$. When the stiffness ratio is large, local deflections become more prevalent and may even be greater than global deflections. Theoretically, an infinite stiffener resistance would prevent any global deformation and only cause local deformation to take place.

The results from the three graphs provide evidence that the model tends toward the correct physical behavior and should be pursued as a possible means of analyzing this very difficult problem.

STRAIN FIELDS AND FRACTURE INITIATION

A criterion for the onset of shell rupture based on the concept of the critical strain to rupture is proposed. With the assumption that axial strain component may be neglected, the tensile strain within each bay is expressed by

$$\varepsilon = \frac{1}{2}(w')^2. \tag{57}$$

For the two-term approximation, the normalized strain distribution in the shell is therefore given as

$$\tilde{\varepsilon} = \frac{1}{2}\tilde{w}_{\tilde{x}}^2, \tag{58}$$

where $\tilde{\varepsilon} = (l/x_o)^2\varepsilon$. The maximum slope occurs at the stiffener and at time $\tilde{t} = \tilde{t}_c$. Substituting values for the first Fourier coefficients, one finds that

$$\tilde{w}_{\tilde{x}}(\tilde{x} = 1, \tilde{t} = \tilde{t}_c) = \frac{-4(2 + \eta)\sin\lambda_1 \cos\lambda_1 \sqrt{(\tilde{I}^2 + \alpha_1^2\lambda_1^2)}}{\lambda_1^2(2 + 3\eta\cos^2\lambda_1)} - 2\alpha_1. \tag{59}$$

A simple fracture criterion such as $\varepsilon \to \varepsilon_c$, where ε_c is a measure of the critical rupture strain, is used to find the condition for first rupture

$$\frac{d}{d\tilde{x}}\tilde{w}(\tilde{x} = 1, \tilde{t} = \tilde{t}_c) = \frac{x_0}{l}\sqrt{2\varepsilon_c} \tag{60}$$

From Eqs. (59) and (60), the following failure criterion is proposed for the stiffened shell

$$\frac{x_0}{l}\sqrt{2\varepsilon_c} = \frac{4(2 + \eta)\sin\lambda_1 \cos\lambda_1 \sqrt{(\tilde{I}_c^2 + \alpha_1^2\lambda_1^2)}}{\lambda_1^2(2 + 3\eta\cos^2\lambda_1)} + 2\alpha_1, \tag{61}$$

where $\tilde{I}_c$ is the critical impulse that would cause the shell to rupture at the stiffener. In the limiting case of $\zeta = \eta$, $\alpha_1 = 0$ and the above criterion reduces to

$$\frac{x_0}{l}\sqrt{2\varepsilon_c} = \frac{4\tilde{I}_c(2 + \eta)\sin\lambda_1 \cos\lambda_1}{\lambda_1^2(2 + 3\eta\cos^2\lambda_1)}. \tag{62}$$

Equations (61) and (62) relate the critical impulse $\tilde{I}_c$ to all other known parameters of the stiffened shell. Equation (62) is converted to physical quantities, and thus a critical impulse to rupture $\bar{I}_c$ is

$$\bar{I}_c = \frac{\lambda_1^2(2 + 3\eta\cos^2\lambda_1)}{4(2 + \eta)\sin\lambda_1 \cos\lambda_1} c\sqrt{2\varepsilon_c}. \tag{63}$$

Note that the critical strain enters the above expression in the power 1/2. Therefore, the critical impulse to rupture depends weakly on ε_c but strongly on geometrical parameters of the problem.

For the general case of $\eta \neq \zeta$, $\bar{I}_c$ depends on the mass and stiffness parameters in a more complex way. The definitions of those parameters involve the length of the bay, the width of the stiffener footing, and the geometry of the ring stiffener. Therefore Eq. (63) can be used to optimize an explosively loaded shell against rupture. This will be the subject of future research.

CONCLUSIONS

A string-on-foundation model has been developed to study the large plastic deformations of a ring-stiffened cylindrical shell undergoing an explosive-type loading. By considering the two main load-resisting mechanisms of a shell undergoing large deformation, longitudinal membrane stretching and circumferential bending, and using an averaging procedure to eliminate the circumferential variable, one reduces the complicated two-dimensional problem to an inhomogeneous partial differential equation in the axial direction and time. The ring stiffeners are represented in this model as discrete springs with their associated stiffness and mass.

Equilibrium is expressed on a local scale by only examining the deformation of the central bay where fracture is most likely to develop. The deformation of the bay is related to the deformation of the adjacent stiffeners through the transmission of shear forces at the interface of the bay and the stiffener. This relationship between the shear forces of the bay and the stiffener is expressed in the boundary condition that is specified at the stiffener. The method of eigenfunction expansion is then used to solve the resulting initial-boundary value problem.

As an example, a ring-stiffened shell subjected to three consecutive underwater explosions is analyzed using the string-on-foundation model. A parametric study on this particular example also shows that interdependencies of a few chosen parameters obey physical reasoning for this problem. The simple model is therefore recommended as a promising new way of analyzing a ring-stiffened shell undergoing explosive loading damage. However, the fluid–solid interaction associated with an underwater explosion needs to undergo further investigation before any reasonable comparison can be made with experimental results. Finally, the model can be used to predict initial shell failure by applying a simple fracture criterion based on the critical strain to rupture.

The work reported herein was supported by the Office of Naval Research under Contract No. N00014-91-J1614 to the University of California, Berkeley, monitored by J. Fein.

REFERENCES

Calladine, C. R., 1977, "Thin-Walled Elastic Shells Analysed by a Rayleigh Method," *International Journal of Solids and Structures,* Vol. 13, pp. 515–530.

Den Hartog, J. P., 1952, *Advanced Strength of Materials,* McGraw–Hill, New York.

Flugge, W., 1973, *Stresses in Shells,* Springer–Verlag, Berlin.

Gurkok, A., and Hopkins, H. G., 1973, "The Effect of Geometry Changes on the Load Carrying Capacity of Beams Under Transverse Load," *SIAM Journal of Applied Mathematics,* Vol. 25, pp. 500–521.

Giovanola, J. H., and Kirkpatrick, S. W., 1992, "Applying a Simple Ductile Fracture Model to Fracture of Welded T-Joints," in the special issue of the ASME AMD Symposium on the Promotion of the Application of Local Fracture/Damage Models to Engineering Fracture Problems, Tempe, AZ, April 28–May 1.

Hoo Fatt, 1992, "Deformation and Rupture of Cylindrical Shells Under Dynamic Loading," Ph.D. thesis, Massachusetts Institute of Technology.

Hoo·Fatt, M. S., and Wierzbicki, T., 1992, "Impact Damage of Long Plastic Cylinders," *International Journal of Offshore and Polar Engineering,* Vol. 2, 147–156.

Huang, J., and Wierzbicki, T., 1993 "Plastic Tripping of Ring Stiffeners," *Journal of Structural Engineering,* Vol. 119.

Kelly, J. M., and Wierzbicki, T., 1967, "Motion of a Circular Viscoplastic Plate Subject to Projectile Impact," *Journal Applied Mathematics and Physics (ZAMP),* Vol. 18, pp. 236–246.

McDonald, W., 1992, "Experimental Results of a Ring-Stiffened Shell Undergoing Underwater Explosive Loading," private communications.

Reid, S. R., 1978, "Influence of Geometrical Parameters on the Mode of Collapse of a 'Pinched' Rigid-Plastic Cylindrical Shell," *International Journal of Solids and Structures,* Vol. 14, pp. 1027–1043.

Stricklin, J. A., Haisler, W. E., and von Reisemann, W. A., 1974, "Large Deflection Elastic-Plastic Response of Stiffened Shells of Revolution," *Journal of Pressure Vessel Technology,* May, pp. 87–94.

Yu, T. X., and Stronge, W., 1990, "Large Deflection of a Rigid-Plastic Beam-on-Foundation from Impact," *International Journal Impact Engineering,* Vol. 9, pp. 115–126.